

SPECTRAL-SPATIAL CLASSIFICATION FROM MULTI-SENSOR COMPRESSIVE MEASUREMENTS USING SUPERPIXELS

Carlos Hinojosa, Juan Marcos Ramirez, Henry Arguello

High Dimensional Signal Processing (HDSP) Group
Universidad Industrial de Santander, Bucaramanga, Colombia

ABSTRACT

Compressive spectral imaging (CSI) acquires coded projections of a spectral image by performing a modulation of the data cube followed by a spectral-wise integration. To avoid the spectral image reconstruction procedure, this paper proposes a classification approach that extracts features directly from multi-sensor CSI measurements. Particularly, the proposed method obtains the features by considering the spectral information extracted from Hyperspectral CSI measurements, and the local spatial information extracted by clustering the Multispectral CSI measurements using a superpixel algorithm. This approach is evaluated on Pavia University and Salinas Valley datasets. Extensive simulations show that considering the local spatial information boosts the overall accuracy up to 3% in comparison with traditional approaches that only uses the spectral information. Furthermore, the computation time of the approach that reconstructs, fuses and classifies takes approximately 87.43 [s], while classifying directly from multi-sensor compressive measurements takes only 0.74 [s], achieving similar classification results.

Index Terms— compressive spectral imaging, multi-sensor measurements, spectral image classification, feature extraction, superpixel algorithms.

1. INTRODUCTION

Spectral imaging senses 2D spatial information along multiple wavelengths. Traditional sensing techniques require scanning all the scene across multiple spectral bands to construct the three-dimensional (3D) data cube [1]. Based on the acquired spectral/spatial resolution, spectral imaging sensors can be categorized in Hyperspectral (HS) and Multispectral (MS). Typically, HS devices capture hundreds of spectral bands of the scene, however, its spatial resolution is often lower compared to that obtained with an MS sensor, which has a low spectral resolution [2]. In this sense, fusion techniques provide a methodological framework for finding a high spatial and spectral resolution image using the information from both HS and MS images [3, 2]. After applying a fusion technique, the spectral signatures (a.k.a spectral pixels) are commonly used as classification features for identifying and detecting different materials within the high-resolution spectral data cube [4, 3, 5, 6, 7].

In general, spectral image classification is a very difficult task due to the inherent data complexity, high storage requirements and

This work was supported by the Vicerrectoría de Investigación y Extensión of the Universidad Industrial de Santander under the Grant 8914: “Strengthening of capacities in applied research through the evaluation, development of technological tools and/or methodologies in the areas of geology and geophysics to reduce exploratory uncertainty in the oil and gas industry”. J. Ramirez was supported by the postdoctoral internship program of the Vicerrectoría de Investigación y Extensión of the Universidad Industrial de Santander.

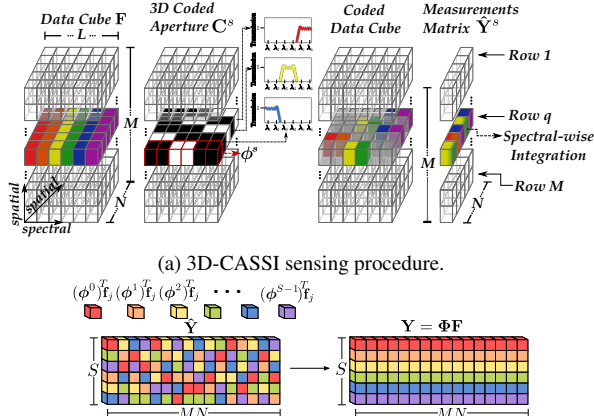
computational costs. Therefore, a preprocessing step to reduce the dimensions of the spectral imagery is often required [8, 9]. On the other hand, compressive spectral imaging (CSI) has recently emerged as a new spectral imaging acquisition approach which captures compressive 2D measurements of the entire data cube rather than directly acquiring all the voxels, hence reducing the data dimensionality [10, 11, 12, 13]. Under the context of CSI, two data fusion algorithms have been recently proposed [14, 15]. In particular, these methods reconstruct a high spatial and spectral resolution image from multi-sensor compressive measurements. Then, an intuitive approach of spectral image classification from multi-sensor compressive measurements would involve two tasks: the reconstruction of the fused image from the HS and MS compressive measurements, and finally, the classification procedure itself. However, this approach implies expensive computational costs and further, the classification accuracy might be degraded due to multiple factors [2, 10].

Although most of the CSI literature has focused on improving the speed and accuracy of the spectral image reconstruction [10, 16, 17, 18], the image recovery stage, in general, is not actually necessary for performing many signal processing tasks [19, 20, 21]. Indeed, the aim of this work is to extract features and perform the spectral image classification directly from multi-sensor compressive measurements without requiring to recover the whole data cube, thus, the CSI reconstruction phase is completely avoided. After acquiring the HS and MS compressive measurements, the proposed method performs a rearrangement and extrapolation procedure from CSI HS measures in order to extract the spectral features. Consecutively, the CSI MS measurements are rearranged before applying a superpixel algorithm [22] in order to obtain the spatial features. Specifically, using this segmentation technique, the proposed method groups pixels with similar spectral characteristics within a nearby neighborhood, incorporating spatial information and hence boosting the classification performance. Finally, the HS and MS extracted features are concatenated before being evaluated in a SVM classifier with a polynomial kernel.

2. PROPOSED METHODOLOGY

2.1. Compressive measurements acquisition

In this work, the 3D-CASSI sensing approach is adopted [13]. In general, denote \mathcal{F} as the spatio-spectral data cube, with $M \times N$ spatial dimensions, L spectral bands and entries denoted as $\mathcal{F}_{m,n,k}$, where m and n index the spatial coordinates, and k determines the k -th spectral band. As shown in Fig. 1 (a), the 3D-CASSI sensing scheme first modulates the voxels of the spectral scene using a 3D coded aperture \mathbf{C}^s , whose entries are indexed as $C_{m,n,k}^s$. Then, the coded spectral scene is integrated in the focal plane array (FPA) detector, along the spectral axis. In CSI it is possible to acquire $S \ll L$



(b) Rearrangement of the matrix $\hat{\mathbf{Y}}$ such that the s -th row of \mathbf{Y} contains the compressive measurements acquired with the s -th coding pattern ϕ^s .

Fig. 1: Acquisition and rearrangement of CSI measurements.

measurement shots, each one employing a different coded aperture, such that different measurements of the spectral data cube are acquired. Therefore, the output of the sensing process, at the (m, n) -th detector pixel and a specific snapshot s , can be expressed as

$$\hat{Y}_{m,n}^s = \sum_{k=0}^{L-1} \mathcal{F}_{m,n,k} C_{m,n,k}^s. \quad (1)$$

Note that for each spatial location of \mathbf{C}^s , it is assigned a coding pattern (optical filter) $\phi^s \in \mathbb{R}^L$, with entries $(\phi^s)_k \in \{0, 1\}$, that modulates a spectral pixel in that particular position before being integrated at the FPA detector. Further, observe that there is a finite number of optical filters randomly distributed in \mathbf{C}^s . In this work, as shown in Fig. 1 (a), the 3D coded apertures are built with non-overlapping optical filters which cover all the spectrum.

The set of compressive measurements from (1) can be arranged in a matrix $\hat{\mathbf{Y}}$ with dimensions $S \times (MN)$, where each column contains the compressive measurements associated to a particular spectral pixel. Note that, each row of $\hat{\mathbf{Y}}$ contains the compressive measurements acquired by the s -th snapshot. However, column vectors of $\hat{\mathbf{Y}}$ contain the spectral pixel measurements in unordered form since, in a particular snapshot, the spectral pixels are encoded using distinct coding patterns. Then, the matrix $\hat{\mathbf{Y}}$ is not convenient for classification as its structure makes difficult to discriminate among compressive measurements. Denoting P as the number of different coding patterns, if the number of measurements shots S equals P , the entries of $\hat{\mathbf{Y}}$ can be rearranged to form a new matrix \mathbf{Y} , such that each row contains the compressed information acquired with a specific coding pattern ϕ^s . Note that this rearrangement is only possible when $S = P$ since in this case it can be guaranteed that, at a specific snapshot, one pixel is encoded only once by a different coding pattern and, at the end of the sensing procedure, all pixels are encoded by the whole set of S coding patterns. Indeed, there are few optical filters in practice hence the case $S = P$ will efficiently extract the information from the underlying data cube. Formally, the rearrangement can be expressed as

$$Y_{s,j} = \hat{Y}_{s',j} \quad \text{if } \hat{Y}_{s',j} = (\phi^s)^T \mathbf{f}_j \quad \forall s',$$

for $s, s' = 0, \dots, S-1$, where $\mathbf{f}_j \in \mathbb{R}^L$ denotes the j -th spectral signature for $j = 0, \dots, MN-1$. This rearrangement, depicted in Fig. 1 (b), preserves the structure of the underlying data improving

the classification results. Alternatively, defining the matrix of S coding patterns as $\Phi = [\phi^0, \phi^1, \dots, \phi^{S-1}]^T$, the problem of acquiring and rearranging the measurements $\hat{\mathbf{Y}}$ can be succinctly expressed as follows

$$\mathbf{Y} = \Phi \mathbf{F}, \quad (2)$$

where $\mathbf{F} \in \mathbb{R}^{L \times (MN)}$ is the spectral image in matrix form, and $\Phi \in \mathbb{R}^{S \times L}$ can be viewed as the projection matrix. In this work the MS (\mathbf{F}_m) and HS (\mathbf{F}_h) images can be modeled from \mathbf{F} as follows:

$$\mathbf{F}_m = \mathbf{D}_m \mathbf{F}, \quad (3)$$

$$\mathbf{F}_h = \mathbf{D}_h \mathbf{F}, \quad (4)$$

where $\mathbf{D}_m \in \mathbb{R}^{L_m \times L}$ and $\mathbf{D}_h \in \mathbb{R}^{MN \times M_h N_h}$ are the spectral and spatial downsampling matrices, with downsampling factor q and p , respectively.

2.2. Features Extraction

2.2.1. HS feature extraction

Following the CSI acquisition model described in Section 2.1, the compressive measurements acquired by the CSI hyperspectral sensor can be succinctly expressed as

$$\mathbf{Y}_h = \Phi_h \mathbf{F}_h, \quad (5)$$

where $\Phi_h \in \mathbb{R}^{S_h \times L}$ is the coding pattern matrix, $\mathbf{Y}_h \in \mathbb{R}^{S_h \times (M_h N_h)}$ contains the compressive measurements in an ordered form, with S_h denoting the number of measurement shots and M_h, N_h the spatial dimensions of the image acquired by the HS CSI sensor.

Although the matrix \mathbf{Y}_h can be used as a feature matrix to perform classification, the goal of this work is to label a high spectral and spatial resolution image taking into account the rich spectral information embedded in \mathbf{Y}_h . Then, a spatial extrapolation is performed by replicating the columns of \mathbf{Y}_h , where the replicated pixels are located to the corresponding high-spatial resolution positions. The extrapolation process can be formulated as follows

$$\omega_h^j = \mathbf{Y}_h^{\left(\lfloor \frac{j'}{p} \rfloor + \frac{M}{p} \left[\lfloor \frac{j'}{M} \rfloor + \lfloor \frac{j'}{Mp} \rfloor \right] \right)}, \quad (6)$$

where ω_h^j is the j -th column of the HS classification features Ω_h ; $\mathbf{Y}_h^{(j')}$ is the j' -th column of the ordered compressive measurements \mathbf{Y}_h ; and $\lfloor x \rfloor$ returns the greatest integer less or equal than x .

2.2.2. MS feature extraction

Similarly, the compressive MS measurements are acquired as

$$\mathbf{Y}_m = \Phi_m \mathbf{F}_m, \quad (7)$$

where $\Phi_m \in \mathbb{R}^{S_m \times L}$ is the coding pattern matrix, whose rows contain the coding patterns of the optical filters used for acquiring the MS compressive measurements. To incorporate the spatial neighborhood information, this work uses a superpixel technique. Superpixel algorithms group pixels into perceptually meaningful atomic regions or segments. This captures image redundancy, provide a convenient primitive from which to compute image features, and greatly reduce the complexity of subsequent image processing tasks. In this work, the segmented image is created by applying the efficient simple linear iterative clustering (SLIC) algorithm [22] on the MS compressive measurements, which are first rearranged back to a $M \times N \times S_m$ image. To reduce the computational cost, before the segmentation,

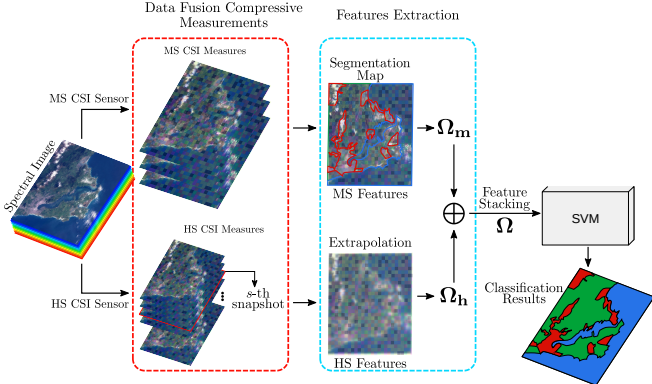


Fig. 2: Workflow of the proposed CSI Spectral-Spatial classification approach.

principal component analysis is applied on the MS compressive measurements and the three principal components are used as the base image for the segmentation. Note that the PCA analysis is only necessary if the number of acquired shots S_m is greater than 3.

Once the segmentation map has been created, it can be utilized with the MS compressive measurements to extract the classification features. Specifically, denote \mathbf{p}^e as the vector containing the indexes of all pixels belonging to the superpixel e , the columns of MS feature matrix Ω_m are created as follows

$$\omega_m^{\mathbf{p}^e} = \frac{\sum_{l=0}^{n_e-1} \mathbf{Y}_m^{(\mathbf{p}^e)_l}}{n_e}, \quad \text{for } e = 0, \dots, N_{seg}, \quad (8)$$

where N_{seg} is the number of segments generated by the superpixel algorithm, $(\mathbf{p}^e)_l$ denotes the l -th entry of the \mathbf{p}^e vector and $\omega_m^{\mathbf{p}^e}$ represents the columns in Ω_m indexed by the vector \mathbf{p}^e . Note that Eq. (8) simply replace all pixels in a segment e by the mean pixel. This procedure incorporates the spatial neighboring information of the superpixel in the classification method.

Finally, the feature matrices obtained from both MS and HS images (Ω_m , Ω_h) are stacked in order to build the feature matrix of the high spatial and spectral resolution image whose columns shall be the input samples of a support vector machines (SVM) classifier. In other words, since the Ω_m and Ω_h have MN columns, the feature matrix is built as $\Omega = [\Omega_h^T, \Omega_m^T]^T$. In this work, the compression ratio is given by $\rho = \frac{S_h + S_m}{L}$. The flowchart of the proposed classification approach from multi-sensor compressive measurements is shown in Fig. 2.

3. SIMULATIONS AND RESULTS

The proposed classification method¹ was first evaluated on the Pavia University dataset, acquired by the Reflective Optics System Imaging Spectrometer (ROSIS-03) sensor [23]. This spectral image consists of 610×340 pixels and 103 spectral bands. In this work, a subset of this spectral image with dimensions $256 \times 256 \times 96$ was used in order to evaluate various classification approaches. Figure 3 (a) shows the ground-truth map of the Pavia University dataset, where each class corresponds to a distinct material in an urban cover. For all the experiments, a SVM classifier is trained using a polynomial kernel and 10% of the samples. In addition, the compression ratio of the acquired CSI measurements is set to $\rho = 25\%$.

¹The MATLAB code along with some simulations can be found in <https://rebrand.ly/icip2019>.

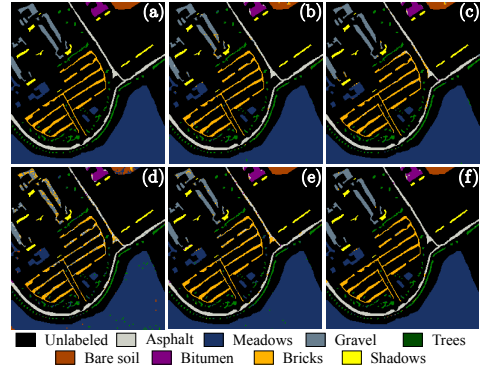


Fig. 3: Classification maps on the Pavia University data set. (a) Ground Truth. (b) Original Image, (c) Reconstruction-Fusion, (d) ACC, (e) Proposed-Noisy, (f) Proposed-Noiseless.

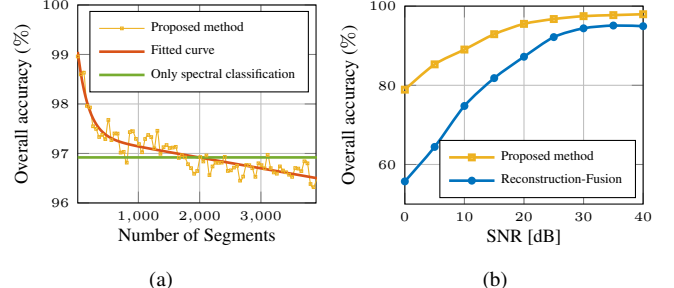


Fig. 4: (a) The overall accuracy of the proposed classification method versus the number of the superpixel segments and (b) the overall accuracy against the SNR of the compressive measurements.

In the first experiment, the number of superpixels is varied in order to analyze the impact of the clustering technique in the overall accuracy (OA). Specifically, Fig. 4 (a) shows the OA versus number of segments (N_{seg}) classification results on the University of Pavia image. As it can be observed, as the number of desired segments increases the overall accuracy decays exponentially, as depicted with the fitted curve in red. In addition, note that, in general, the proposed method outperforms the spectral classification over the original image when using $N_{seg} \leq 1600$. Indeed, it can be seen from the figure that the incorporation of spatial neighboring information boost the classification accuracy up to 3% in OA, when the chosen number of superpixels is approximately the number of classes within the spectral scene. Therefore, the number of segments is fixed to $N_{seg} = 10$ for the subsequent experiments on the Pavia University dataset.

It is important to note that the measurements described by Eq. (2), in general, are noise free. However, in real CSI architecture, the compressive measurements are contaminated with noise due to the physical limitation of the sensor and imperfections of the acquisition system. Therefore, Eq. (2) should be rewritten as $\mathbf{Y} = \Phi \mathbf{F} + \Sigma$, where $\Sigma \sim N(0, \sigma^2)$ represents the noise of the system. Figure 4 (b) shows the overall accuracy results of the proposed classification method versus the SNR of compressive measurements. For comparison purposes, the accuracy results of the Reconstruction-Fusion method is included in Fig. 4 (b). As can be seen in this figure, the proposed method outperforms the other method for the test interval.

Figures 3 (b), (c), (e) and (f) show the classification maps obtained when the SVM is applied on the original spectral image (Original Image), a reconstructed and fused spectral image from compressive measurements (Reconstruction-Fusion), the extracted features (Ω) from noisy compressive measurements (Proposed-

Table 1: Performance of the various classification approaches on the Pavia University dataset.

Class	Original-image	Reconstruction-Fusion	ACC Framework	Proposed-Noisy	Proposed-Noiseless
Asphalt	86.80 ± 2.03	84.62 ± 1.05	91.20 ± 1.21	95.05 ± 4.62	98.63 ± 0.70
Meadows	99.07 ± 0.02	99.23 ± 0.22	95.78 ± 0.14	98.95 ± 0.17	99.77 ± 0.02
Gravel	82.39 ± 1.35	80.03 ± 6.67	79.62 ± 0.31	78.04 ± 4.58	99.67 ± 0.16
Trees	88.61 ± 2.41	91.55 ± 2.62	92.06 ± 0.27	86.86 ± 3.13	93.35 ± 0.07
Bare-Soil	61.96 ± 5.89	72.45 ± 5.89	85.57 ± 0.98	88.98 ± 6.46	98.25 ± 2.47
Bitumen	93.29 ± 0.97	90.82 ± 2.51	77.11 ± 0.16	93.70 ± 3.10	92.19 ± 0.97
Self-Block Bricks	90.40 ± 0.20	85.14 ± 3.19	83.16 ± 0.24	83.05 ± 1.19	97.58 ± 1.03
Shadows	100.00 ± 0.00	99.89 ± 0.15	98.47 ± 0.66	98.42 ± 0.74	98.74 ± 0.00
OA (%)	94.51 ± 0.35	94.05 ± 0.72	90.88 ± 0.43	94.55 ± 0.60	98.90 ± 0.03
AA (%)	87.81 ± 1.26	87.97 ± 0.01	87.87 ± 1.05	90.38 ± 0.86	97.27 ± 0.40
κ	0.91 ± 0.0062	0.90 ± 0.0119	0.88 ± 0.0147	0.91 ± 0.0105	0.98 ± 0.0005
Time (s)	1.17 ± 0.007	87.43 ± 1.77	24.97 ± 2.35	0.66 ± 0.050	0.74 ± 0.037

Noisy), and the extracted features from noiseless compressive measurements (Proposed-Noiseless), respectively. In addition, the proposed method was compared with the Adaptive Compressed Classification (ACC) framework [24], using SVM, in Fig. 3 (d). For the Reconstruction-Fusion classification approach, we implement the spectral image reconstruction method developed in [16] and the coupled nonnegative matrix factorization (CNMF) fusion technique [25]. For the Proposed-Noisy approach, the proposed method is applied to noisy compressive measurements with SNR = 25 dB.

In order to further validate the performance of the proposed approach, quantitative results are presented for the selected spectral scene in Table 1. All the presented results are the average of 10 experiments, each with different realizations of Φ_h and Φ_m coding patterns, and the best value of each row is shown in bold font. Furthermore, Table 1 shows the numerical results for each of the eight land-cover classes (producer's accuracy), overall accuracy (OA), average accuracy (AA), Kappa (κ) coefficients [26] and time. All the results, except the Kappa coefficients, are given in percentage.

From the Table 1, it can be clearly observed that the proposed classification approach provide comparable results to applying the method directly on the original and reconstructed spectral data cube. In addition, performing the classification directly on the CSI measurements is significantly faster than performing all the processing in the complete and the reconstructed spectral data. As observed, the results show that when no noise is assumed, the achieved classification accuracy outperforms the results obtained with the full spectral data cube. As reported in some works, random projections are not sensitive to impulse noise thus can be used as a noise reduction method [27]. In other words, the achieved results when using noise-free compressive measurements are due to the random projection, described in Eq. (2), removes noise from the acquired measurements. Finally, as clearly observed from Table 1, ACC is outperformed by the proposed method in both, noisy and noiseless case.

For the sake of completeness, we evaluate the proposed method on the Salinas dataset, captured by the Airborne Visible/Infrared Imaging Spectrometer (AVIRIS) [23]. This image has dimensions of 512×217 pixels and 204 spectral band. In this work, a subset of $217 \times 217 \times 192$ is used to evaluate the proposed classification method. Fig. 5(a) shows an RGB composite of the Salinas Valley spectral image and Fig. 5(b) shows the ground truth map of eight land-cover classes corresponding to different kinds of crops. Moreover, Fig. 5(c)-(f) show the classification maps obtained from the original image, the Reconstruction-Fusion approach, the proposed method using noisy compressive measurements (Proposed-Noisy), and the proposed method using noiseless compressive measurements (Proposed-Noiseless), respectively. As can be observed in these figures, the classification map generated by the proposed method over noiseless compressive measurements exhibits a superior per-

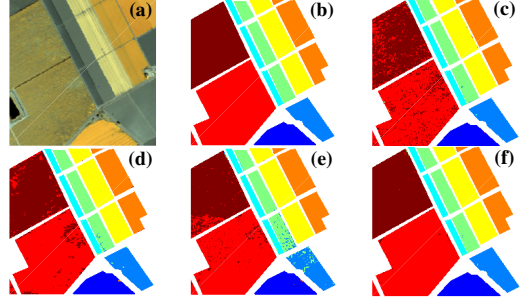


Fig. 5: Salinas Valley dataset: (a) RGB composite of the spectral image, (b) Ground Truth, (c) Original Image, (d) Reconstruction-Fusion, (e) Proposed-Noisy, (f) Proposed-Noiseless.

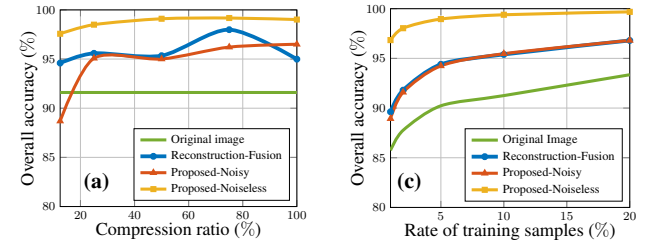


Fig. 6: (a) The overall accuracy on the Salinas Valley dataset versus the compression ratio and (b) the overall accuracy versus the rate of training samples.

formance compared with those yielded by the other approaches.

Figure 6 (a) shows the overall accuracy versus the compression ratio for the various classification approaches. Each point of these curves is obtaining by averaging 20 realizations of the respective experiment, and for each trial, a new set of colored coded apertures is built and a random set of training samples are selected. Furthermore, the rate of training samples is set to 10% and the number of super-pixels is fixed to $N_{seg} = 10$. As can be seen in this figure, the proposed classification approach using noiseless measurements has a remarkable performance in comparison with the other methods. Finally, Fig. 6 (b) shows the overall accuracy as the rate of training samples increases. As can be observed in this figure, the proposed method from noiseless measurements outperforms the other classification approaches for the entire evaluation interval, achieving an accuracy gain of at least 3%.

4. CONCLUSIONS

This work presented a spectral-spatial image classification approach, which perform all the processing tasks directly on multi-sensor compressive measurements. The proposed method performs a superpixel algorithm with the multispectral CSI measures in order to incorporate spatial neighboring information in the classification features. In addition, spectral and some spatial features are extracted from the hyperspectral CSI measures, using an extrapolation procedure. The proposed approach was validated through some preliminary experiments. In general, the results show that performing the classification directly on the compressive measurements provides similar accuracy results, in a lesser time, compared with those provided by performing the classification on the original 3D spectral image and the reconstructed image pixels. Particularly, a maximum difference of approximately 4% in terms of OA was observed when comparing the classification results obtained using the original image with those achieved using the CSI multi-sensor measurements acquired with the 3D-CASSI sensing scheme.

5. REFERENCES

- [1] Gary A Shaw and Hsiao-Hua K Burke, "Spectral imaging for remote sensing," *Lincoln Laboratory Journal*, vol. 14, no. 1, pp. 3–28, 2003.
- [2] Naoto Yokoya, Claas Grohnfeldt, and Jocelyn Chanussot, "Hyperspectral and multispectral data fusion: A comparative review of the recent literature," *IEEE Geoscience and Remote Sensing Magazine*, vol. 5, no. 2, pp. 29–56, 2017.
- [3] Pedram Ghamisi, Naoto Yokoya, Jun Li, Wenzhi Liao, Sicong Liu, Javier Plaza, Behrood Rasti, and Antonio Plaza, "Advances in hyperspectral image and signal processing: A comprehensive overview of the state of the art," *IEEE Geoscience and Remote Sensing Magazine*, vol. 5, no. 4, pp. 37–78, 2017.
- [4] Pedram Ghamisi, Javier Plaza, Yushi Chen, Jun Li, and Antonio J Plaza, "Advanced spectral classifiers for hyperspectral images: A review," *IEEE Geoscience and Remote Sensing Magazine*, vol. 5, no. 1, pp. 8–32, 2017.
- [5] Lin He, Jun Li, Chenying Liu, and Shutao Li, "Recent advances on spectral–spatial hyperspectral image classification: An overview and new guidelines," *IEEE Transactions on Geoscience and Remote Sensing*, vol. 56, no. 3, pp. 1579–1597, 2018.
- [6] Carlos A. Hinojosa, Jorge Bacca, and Henry Arguello, "Spectral imaging subspace clustering with 3-d spatial regularizer," in *Imaging and Applied Optics 2018 (3D, AO, AIO, COSI, DH, IS, LACSEA, LS&C, MATH, pcAOP)*. 2018, p. JW5E.7, Optical Society of America.
- [7] Karen Sanchez, Carlos Hinojosa, and Henry Arguello, "Supervised spatio-spectral classification of fused images using superpixels," *Appl. Opt.*, vol. 58, no. 7, pp. B9–B18, Mar 2019.
- [8] Wei He, Hongyan Zhang, Liangpei Zhang, Wilfried Philips, and Wenzhi Liao, "Weighted sparse graph based dimensionality reduction for hyperspectral images," *IEEE Geoscience and Remote Sensing Letters*, vol. 13, no. 5, pp. 686–690, 2016.
- [9] B. Rasti, M. O. Ulfarsson, and J. R. Sveinsson, "Hyperspectral feature extraction using total variation component analysis," *IEEE Transactions on Geoscience and Remote Sensing*, vol. 54, no. 12, pp. 6976–6985, Dec. 2016.
- [10] Gonzalo R Arce, David J Brady, Lawrence Carin, Henry Arguello, and David S Kittle, "Compressive coded aperture spectral imaging: An introduction," *IEEE Signal Processing Magazine*, vol. 31, no. 1, pp. 105–115, 2014.
- [11] Carlos Hinojosa, Henry Arguello, and Hoover Rueda, "Analysis of matrix completion algorithms for spectral image estimation from compressive coded projections," in *2015 20th Symposium on Signal Processing, Images and Computer Vision (STSIVA)*. IEEE, 2015, pp. 1–7.
- [12] Claudia V Correa, Carlos Hinojosa, Gonzalo R Arce, and Henry Arguello, "Multiple snapshot colored compressive spectral imager," *Optical Engineering*, vol. 56, no. 4, pp. 041309, 2016.
- [13] Xun Cao, Tao Yue, Xing Lin, Stephen Lin, Xin Yuan, Qionghai Dai, Lawrence Carin, and David J Brady, "Computational snapshot multispectral cameras: Toward dynamic capture of the spectral world," *IEEE Signal Processing Magazine*, vol. 33, no. 5, pp. 95–108, 2016.
- [14] E. Vargas, Ó. Espitia, H. Arguello, and J. Tourneret, "Spectral image fusion from compressive measurements," *IEEE Transactions on Image Processing*, vol. 28, no. 5, pp. 2271–2282, May 2019.
- [15] E. Vargas, H. Arguello, and J. Tourneret, "Spectral image fusion from compressive measurements using spectral unmixing and a sparse representation of abundance maps," *IEEE Transactions on Geoscience and Remote Sensing*, pp. 1–11, 2019.
- [16] Henry Arguello and Gonzalo R Arce, "Colored coded aperture design by concentration of measure in compressive spectral imaging," *IEEE Transactions on Image Processing*, vol. 23, no. 4, pp. 1896–1908, 2014.
- [17] Hans Garcia, Claudia V Correa, and Henry Arguello, "Multi-resolution compressive spectral imaging reconstruction from single pixel measurements," *IEEE Transactions on Image Processing*, vol. 27, no. 12, pp. 6174–6184, 2018.
- [18] Nelson Diaz, Carlos Hinojosa, and Henry Arguello, "Adaptive grayscale compressive spectral imaging using optimal blue noise coding patterns," *Optics & Laser Technology*, vol. 117, pp. 147–157, 2019.
- [19] Mark A Davenport, Petros T Boufounos, Michael B Wakin, and Richard G Baraniuk, "Signal processing with compressive measurements," *IEEE Journal of Selected Topics in Signal Processing*, vol. 4, no. 2, pp. 445–460, 2010.
- [20] Wei Li, Saurabh Prasad, and James E Fowler, "Classification and reconstruction from random projections for hyperspectral imagery," *IEEE Transactions on Geoscience and Remote Sensing*, vol. 51, no. 2, pp. 833–843, 2013.
- [21] C. Hinojosa, J. Bacca, and H. Arguello, "Coded aperture design for compressive spectral subspace clustering," *IEEE Journal of Selected Topics in Signal Processing*, vol. 12, no. 6, pp. 1589–1600, Dec 2018.
- [22] Radhakrishna Achanta, Appu Shaji, Kevin Smith, Aurelien Lucchi, Pascal Fua, Sabine Süsstrunk, et al., "Slic superpixels compared to state-of-the-art superpixel methods," *IEEE transactions on pattern analysis and machine intelligence*, vol. 34, no. 11, pp. 2274–2282, 2012.
- [23] Computational Intelligence Group (GIC), "Hyperspectral remote sensing scenes," [Online]. Available: http://www.ehu.eus/ccwintco/index.php?title=Hyperspectral_Remote_Sensing_Scenes.
- [24] Jurgen Hahn, Simon Rosenkranz, and Abdelhak M Zoubir, "Adaptive compressed classification for hyperspectral imagery," in *Acoustics, Speech and Signal Processing (ICASSP), 2014 IEEE International Conference on*. IEEE, 2014, pp. 1020–1024.
- [25] N. Yokoya, T. Yairi, and A. Iwasaki, "Coupled nonnegative matrix factorization unmixing for hyperspectral and multispectral data fusion," *IEEE Transactions on Geoscience and Remote Sensing*, vol. 50, no. 2, pp. 528–537, Feb. 2012.
- [26] Humboldt State University Geospatial [Online], "Introduction to remote sensing: Accuracy metrics," <https://goo.gl/vK2KKj>.
- [27] Ella Bingham and Heikki Mannila, "Random projection in dimensionality reduction: applications to image and text data," in *Proceedings of the seventh ACM SIGKDD international conference on Knowledge discovery and data mining*. ACM, 2001, pp. 245–250.